Journal of Materials Chemistry A

Accepted Manuscript

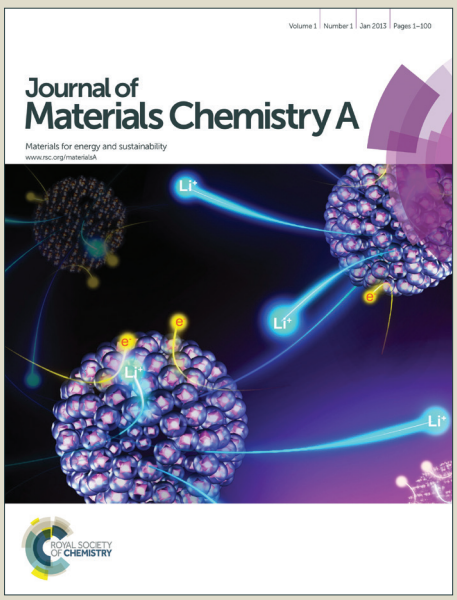

ROYAL SOCIETY OF CHEMISTRY

www.rsc.org/materialsA

Activated carbon-based gas sensors: Effects of surface features on sensing mechanism

Nikolina A. Travlou[1], Mykola Seredych[1], Enrique Rodriguez-Castellon[2] and Teresa J. Bandosz[1]*

[1]*Department of Chemistry, The City College of New York*

160 Convent Ave, New York, NY, 10031, USA.

[2]*Departamento de Química Inorgánica, Facultad de Ciencias, Universidad de Málaga, 29071 Málaga, Spain*

**Corresponding author: E-mail: tbandosz@ccny.cuny.edu; Fax: +1 212 650 6107; Tel: +1 212 650 6017*

Table of contents entry

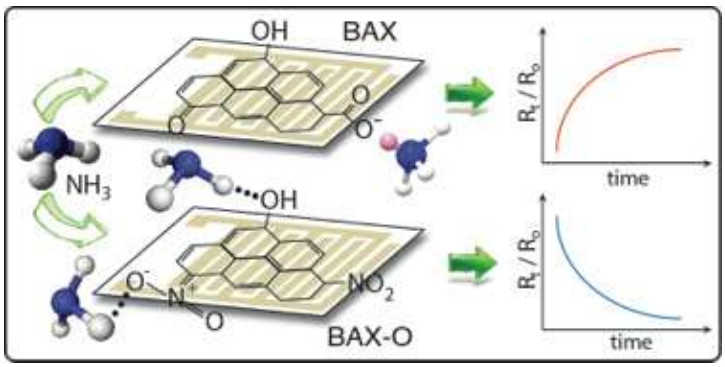

Activated carbon chips show great potential for ammonia detection with an adsorption-based reversible sensing mechanism depending on carbon surface chemistry.

Abstract

Ammonia sensing capability of a commercial wood-based activated carbon (BAX) and its oxidized counterpart (BAX-O) was studied. The materials were exposed to continuous cycles of various ammonia concentrations, followed by purging with air, and changes in normalized resistance were analyzed. When initially exposed to the reducing gas, chemical interactions between ammonia and the carbons generated an irreversible signal change, which was stronger in the case of the initial carbon. After equilibration and reactive adsorption the sensors were further tested with ammonia. During the reversible sensing, the two carbons exhibited opposite trends in their signal. This indicates that oxidation changed the electrical properties of the carbon sample, leading to a different sensing mechanism. For the initial material holes play the predominant role in current transport, while their depletion upon exposure to the reducing gas, leads to a decrease in the conductivity. In the case of oxidized sample, the presence of electron donating nitro groups causes hole annihilation in the carbon itself converting it to a predominantly n-type material. Here exposure to ammonia, increases the conductivity of the chip owing to the electron donating properties of the gas. Physical interactions such as hydrogen bonding, polar interactions with the surface functional groups, and dispersive interactions of ammonia with the carbon matrix, led to the pore filling govern the extent of the response signal. The sensor signal changes linearly with the ammonia concentration.

Key words: gas sensors, activated carbons, oxidation, ammonia adsorption

Introduction

Ammonia (NH_3) is a toxic gas, which is most commonly used by fertilizer industry. It is released to environment as a byproduct of fossil fuel combustion,[1] metabolic processes[2,3] and anaerobic digestion. While exposure to ammonia at low levels such as 100 ppm can irritate the respiratory tract, it is poisonous and may be fatal if inhaled in even greater concentrations. The US Occupational Safety and Health Administration (OSHA) has set a permissible exposure limit of 50 ppm over a conventional 8-h work day or a 40-h work week, and a short-term exposure limit (STEL) of 35 ppm, for ammonia vapor in ambient conditions.[4,5] The National Institute for Occupational Safety and Health (NIOSH) recommends a limit of 300 ppm of ammonia for 30 to 60 minutes, which is based on acute inhalation toxicity, and is considered as immediately dangerous to life or health (IDLH).[5–7] Hence, ammonia detection at low concentrations is of paramount importance for human health. Furthermore, the precise detection limits of ammonia may contribute to the improvement of monitoring systems of ambient ammonia levels and disease diagnosis as a result of which ammonia is given off.[8,9]

The evaluation of the performance of a gas sensor is based on several factors. These include the selectivity of a sensor, which is connected with the ability to distinguish a specific gas among others, its sensitivity, that indicates the smallest detectable absolute amount of change, its response time, which is the necessary time for a sensor to change output state when an input parameter change occurs, and its reversibility that indicates the ability of the system to return to its original state after a detection. Finally, an additional crucial factor that defines the sensitivity and selectivity of a sensor is its affinity to interact with a toxic gas,[10] which might be affected by its adsorption capacity.

A significant number of studies have been reported on nanoscale carbon-based materials for gas detection. Carbon nanotubes, exfoliated graphene sheets, graphitic nanoribbon films and graphite oxide for instance, have proven to have a very high sensitivity to different gases, including ammonia.[9,11–20] A sensing mechanism of these carbon-based materials toward reducing gases such as ammonia, is based on a decrease in the conductivity, which is consistent with p-type doping.[11–16] In the case of these sensing materials, under ambient conditions, holes play a predominant role in a charge transfer. When exposed to reducing gases such as ammonia, an increase in their resistance is related to the hole depletion of the sensing material. Even though all of these carbon-based materials are very sensitive, they are not selective toward different reducing gases. Hence, for the improvement of their selectivity, functionalization processes are required in many cases.[12,21,22]

In previously reported carbon-based sensor studies, it has been shown that single and multiwall carbon nanotubes (SWCNT and MWCNTs) functionalized with nanoparticles (NPs) such as Au, Pd and Ag,[23] or (MWCNTs)–polymer composite-based hybrid gas sensors,[24] exhibit improved selectivity toward specific gases, as well as improved electrical response. Abdelhalim and co-workers examined the response of a CNT-based gas sensor functionalized with Au, toward different ammonia concentrations, varying from 10 -100 ppm. They found that upon exposure to 100 ppm of the target gas, the sensor reached normalized response of 92%.[24] Similar to CNT-based sensors, graphene and reduced graphene oxide have proven to be promising candidates toward the detection of reducing gases, such as NH_3. However, their functionalization with metals,[25] and conducting polymers such as polyaniline (PANI),[19] lead to their improved selectivity and greater electrical response, compared to those sensors that were not functionalized. Huang and co-workers studied an ammonia gas sensor based on reduced

graphene oxide (RGO)-polyaniline (PANI) hybrids, and showed that while the unmodified RGO-based sensor exhibited about 5.2% change in the normalized resistance when exposed to 50 ppm of ammonia. When used for the same ammonia concentration, the hybrid material exhibited an improved response of 59.2%.[19] Wang and co-workers fabricated an ammonia gas sensor based on chemically reduced graphene oxide with pyrrole vapor, Py-rGO. The response of the sensor was examined at various ammonia concentrations ranging from 5 ppb to 100 ppm, and it was shown that the sensor exhibited about 4.2% increase in the normalized resistance upon exposure to 5 ppb of the target gas, and about 22% increase upon exposure to 100 ppm.[26]

Simultaneously, in recent years, carbon-based materials have been evaluated from the view point of their transition from n-type to p-type materials, and their second conversion to n-type, upon annealing.[27] It was shown that these conduction conversions are related to the formation of acceptor defects that are responsible for the first p-type conversion, and donor defects that cause the second n-type conversion. It has also been reported that graphene nanoribbons under functionalization by nitrogen species through high-power electrical joule heating in ammonia, exhibit n-type electronic doping.[28]

Activated carbons, which are widely used for various gas separation processes, despite their limited conductivity compared to CNTs, exhibit certain advantages which might contribute to their application as gas sensors.[29,30] Among them, a developed internal porous structure, extensive surface area, rich surface chemistry, possibility of tailoring their structure for particular applications, chemical stability and favorable price, are some of the most striking ones.[31,32] The chemical and structural properties of activated carbons, which determine the adsorptive properties, depend on the nature of the precursor as well as the process and conditions that are applied during the preparation procedure.[33,34]

In our previous study,[35] ammonia sensing was addressed on chips made of sulfur-doped synthetic nanoporous carbons. It was shown that such carbons can operate both as ammonia detectors because of their sensing ability, and also as protectors against the toxic gas, due to their ability to remove ammonia through the adsorption process. Therefore, the objective of this paper is to examine the sensing response of commercial wood-based activated carbons to various ammonia concentrations, and to demonstrate how the surface chemistry and porosity of these materials is related to the adsorption mechanism and hence the electrical response of the sensor. For the initial testing, a wood-based activated carbon of micro/mesoporous structure has been chosen. Although these carbons have previously been studied as NH_3 adsorbents,[30,36] the extensive characterization of the new batch used in this study will be presented here to derive the sensing mechanism and to account for differences in the materials' properties. The detection behavior and response time of the activated carbons are examined for different ammonia concentrations in the range between 10 to 500 ppm. Since adsorption is the principle of gas sensing on these materials, they can also contribute to personal protection against that toxic gas.

Results and Discussion

Fig. 1 demonstrates the normalized resistance changes ($R_t\ R_o^{-1}$) of BAX and BAX-O when initially exposed to 100 ppm of ammonia and then recovered in air. BAX and BAX-O coated microchips have a resistance of 68 kΩ and 1.04 MΩ, respectively. Even though the resistivity of the systems is high, it has the potential to provide a measurable electrical signal during the sensing procedure.

The differences in the responses of both carbons, are clearly seen. BAX exposed to ammonia, exhibits a 27% gradual increase in the resistance, while it takes one hour for the signal to reach a plateau, which we associate with the adsorption equilibrium. BAX-O on the other hand, exhibits a 60% decrease in the resistance when exposed to ammonia and requires less than 30 minutes to reach the equilibrium.

The microchips were initially exposed to ammonia assuming that this process will result in the exhaustion of all reactive sites. After reaching a stable signal, ammonia was turned off and the sensor was purged with air to remove the physically adsorbed gas, and to determine the role of chemisorption (irreversible processes) and porosity on the extent of the sensing signal. That process lasted until the system reached plateau in the electrical response. As expected, a change in the signal was found, but once again it followed different trend for each sample. While for BAX, normalized resistance decreased 12 %, for BAX-O it increased 20 %. These results indicate that the interactions that generate the irreversible signal, are probably stronger in the case of the initial carbon, and this hypothesis will be further supported by the chemical analyses and porosity data.

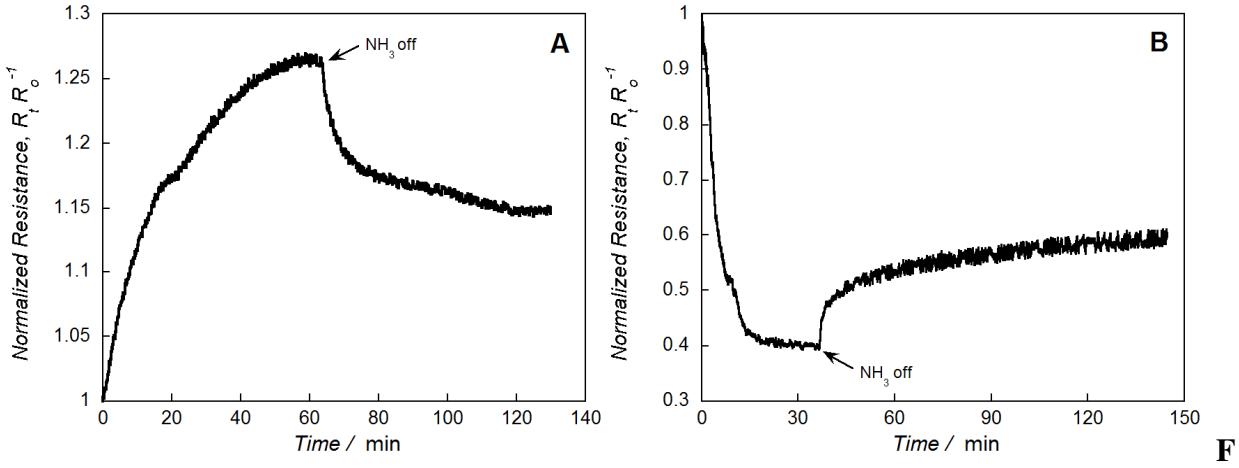

ig. 1. Normalized change in resistance of BAX (A) and BAX-O (B) upon initial exposure to ammonia and subsequent purging with air after stabilization.

After the initial exposure, the activated-carbon based sensors were further tested to explore the reversible sensing, which is an important feature of gas sensors. For this purpose the chips were exposed to different ammonia concentrations, varying from 100 to 500 ppm. The sensor response was also examined for lower ammonia concentrations (20 ppm and 10 ppm). However, due to the different response time of the sensor upon exposure to lower concentrations of the target gas, the sensing cycles for 20 ppm and 10 ppm will be presented and discussed later in this paper.

The change in the normalized resistance upon the exposure to different concentrations is presented in Fig. 2 and Table 1. It is clearly seen that when BAX and BAX-O are exposed to continuous cycles of NH_3 adsorption/desorption, they demonstrate good consistency and reversibility of the response. When these chips are purged with air, ammonia is apparently removed. Thus the sites that took part in reversible adsorption during the exposure, become again available to interact with the gas, causing a change in the electrical property of the carbons. However, once again, both samples seem to exhibit opposite signal trends.

Table 1. Change in the normalized resistance ($R_t\ R_0^{-1}$) of BAX and BAX-O after exposure to various ammonia concentrations.

NH_3 concentration (ppm)	$R_t R_0^{-1}$, (%)	
	BAX	BAX-O
100	15.7	14.2
175	19.9	16.8
250	22.2	19.7
375	27.2	22.5
500	29.2	24.9

Considering that the activated carbons addressed here were not functionalized with metal nanoparticles, metal oxides or polymers, the electrical response of our sensors is relatively high, compared to the performance of other non-functionalized graphene based sensors, where much smaller electrical signal changes were recorded upon exposure to ammonia.[19, 37-39] When RGO was used, the sensor exhibited 5.2% change of the normalized resistance upon exposure to 50 ppm of ammonia.[19] Yavari and co-workers used a macroscopic three-dimensional graphene network for NH_3 detection and their sensor upon exposure to 1000 ppm ammonia exhibited ~ 30% resistance change, while at 20 ppm, it exhibited a change smaller than 4%.[37] In another study multi-walled carbon nanotubes (MWCNTs)-polymer composite-based hybrid sensors presented sensitivity of 28% when exposed to 100 ppm of ammonia. For the preparation of the hybrid materials, polymers such as PEDOT:PSS (poly(3,4-ethylenedioxythiophene)-polystyrene sulfonic acid) and PANI (polyaniline), were used.[24] M. Gautam and A.H. Jayatissa examined a graphene-based ammonia gas sensor, functionalized with Au nanoparticles. Its response was

studied in ammonia concentrations varying from 15 ppm to 58 ppm, and it was found as 8% and 35%, when exposed to 58 ppm and 15 ppm of the target gas, respectively.[38]

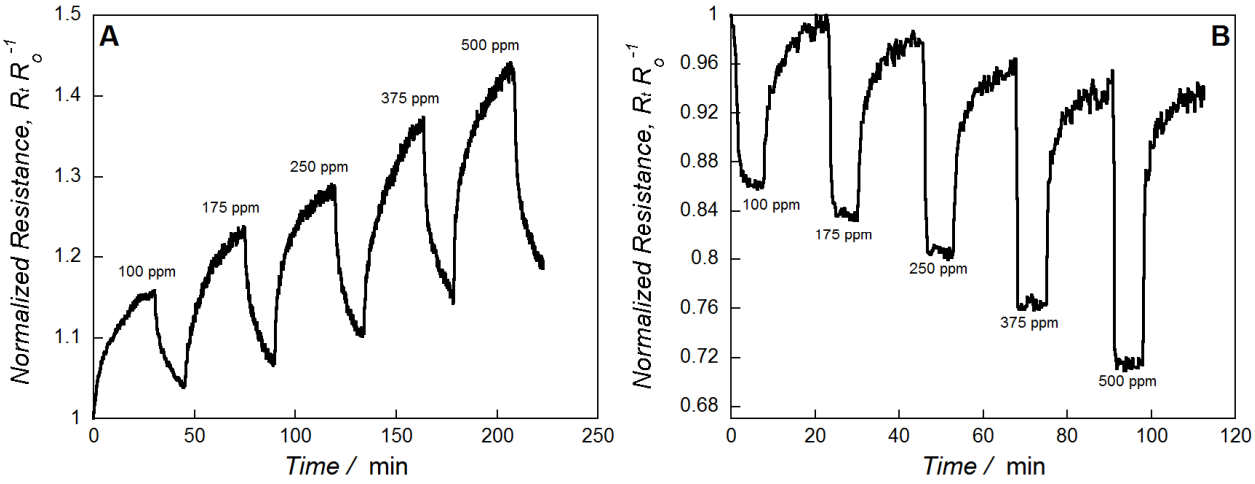

Fig. 2. Response curve for BAX (A) and BAX-O (B) both at various ammonia concentrations.

To understand the observed trends in the sensing behavior, the surface of the initial and exhausted samples was extensively characterized. Although BAX and BAX-O have previously been studied as NH_3 adsorbents,[30,36,40] the particular batch used in this study was analyzed, in order to derive the sensing mechanism and to account for differences in the materials' properties.

Table 2. Ammonia breakthrough capacity and surface pH values

	NH_3 breakthrough capacity	pH	
sample	(mg g^{-1} of adsorbent)	Initial	Exhausted
BAX	11.5	6.52	7.06
BAX-O	30.7	3.47	5.33

In a previous study,[36] it has been shown that the capacity of these carbons for ammonia retention is affected by the type of surface functional groups. Especially strongly acidic groups

were found to enhance NH_3 adsorption capacity via acid-base interactions. The ammonia breakthrough capacity curves of our materials along with the calculated breakthrough capacities and pH values of the carbon surfaces are presented in Fig. S1 of Supplementary Information and in Table 2, respectively. As seen, the performance of the carbons differs, with BAX exhibiting a shorter breakthrough time compared to BAX-O. Even though the capacity values are not very high compared to those of modified carbons,[41] chemical oxidation resulted in an almost threefold increase in their performance toward ammonia removal. This trend of the capacity values is in agreement with those reported for the majority of carbons, where a larger amount of oxygen acidic groups and a higher porosity from oxidation, enhances ammonia adsorption.[36] An enhancement in these parameters is also expected for our carbons. Looking at the pH values (Table 2), it is seen that the initial carbon is almost neutral, while oxidation with HNO_3 led to a significant decrease in the surface pH. After ammonia adsorption, the pH value increased only slightly for the BAX sample, which is linked to the small amount adsorbed. On the other hand, for BAX-O an increase of a few pH units indicates that a larger amount of ammonia is adsorbed on the carbon or reacts with the surface acidic groups.

The parameters of the porous structure and the pore size distributions for BAX and BAX-O, before and after exposure to ammonia, are summarized in Table 3 and Fig. S2 of Supplementary Information, respectively. As seen, BAX has a surface area of 1549 m^2 g^{-1} and significant volumes of mesopores and micropores. After oxidation the volumes of these pores decreased 30% and 11%, respectively. On the other hand, the volume of ultramicropores increased 28%. Here, an increase in the volume of pores smaller than 0.7 nm, where the physical adsorption of ammonia should be the strongest, is the most significant (71%). The total surface

area of the oxidized sample decreased to 1408 m^2 g^{-1}. Thus an increase in the volume of ultramicropores might contribute to the increased adsorption capacity.

Table 3. The parameters of porous structure for BAX and BAX-O before and after exposure to ammonia.

Sample	S_{NLDFT} (m^2 g^{-1})	$V_{<0.7nm}$ (cm^3 g^{-1})	$V_{<.1nm}$ (cm^3 g^{-1})	V_{mic} (cm^3 g^{-1})	V_{meso} (cm^3 g^{-1})	V_t (cm^3 g^{-1})	V_{micro} /V_t
BAX	1549	0.086	0.225	0.617	0.756	1.373	0.45
BAX-O	1408	0.147	0.252	0.551	0.531	1.082	0.51
BAX-E	1616	0.090	0.232	0.648	0.793	1.441	0.45
BAX-O-E	1427	0.137	0.259	0.556	0.532	1.088	0.51

Exposure to ammonia didn't cause any significant change in the volume of micropores, ultramicropores and mesopores for the oxidized sample. This indicates that physisorption rather than chemisorption is the predominant mechanism for gas sensing on BAX-O. Reactive adsorption of ammonia and formation of stable surface compounds would probably lead to a change in the pore volume.[41] This is seen in the case of BAX, where, even though the volumes of micropores, ultrananopores and mesopores do not significantly change after ammonia adsorption, still a small increase in the volume of micropores and mesopores are likely caused by some degree of chemisorption that takes place. The pore size distributions are presented in Fig. S2 of Supplementary Information. They indicate that for both carbons the volume of pores smaller than 1 nm increased after the dynamic adsorption process which might be due to a decrease in the apparent size of the pores, as a result of reactive adsorption. SEM images presented in Fig. S3 of Supplementary Information show highly porous structures for both carbons. No significant differences in the texture were found.

The Raman spectra for BAX and BAX-O are presented in Fig. S4 of Supplementary Information. The G and D bands are found at 1596 cm^{-1} and at 1355 cm^{-1}, respectively. The latter one indicates the presence of defects. An increase in the defects caused by oxidation is seen in an increase in the intensity ratio of D to G bands (I_D/I_G), from 0.75 for BAX to 0.81 for BAX-O.

Table 4. Content of elements on the surface (in at. % from XPS analysis and in wt. % from CHN analysis).

	XPS (at. %)					CHN (wt. %)			
Sample	C	O	N	P	Na	C	O	N	H
BAX	89.2	9.1	0.6	0.9	0.24	84.4	13.2	0.3	2.2
BAX-E	92.5	6.4	0.6	0.5	---	82.6	14.3	0.5	2.5
BAX-O	79.8	`17.3	2.6	0.3	---	68.8	25.6	2.5	3.2
BAX-OE	79.9	16.9	2.7	0.4	---	70.5	23.4	2.6	3.5

XPS analysis was carried out, in order to better understand the nature of the functional groups present on the carbon surfaces and their effect on ammonia adsorption. The content of elements in atomic % and the results of the deconvolution of the C 1*s*, O 1*s* and N 1*s* are given in Tables 4 and 5, respectively. The deconvolution of C 1*s* and O 1*s* core energy levels for the initial and exposed to ammonia carbons are presented in Fig. S5 and Fig. S6 of Supplementary Information. As expected, after oxidation the total oxygen and nitrogen contents increased. The latter is attributed to the effect of the nitrogen presence in the oxidizing agent (HNO_3).

A close look at the deconvolution of N 1*s* core energy levels (Fig. 3) and the XPS [at. %] suggests that BAX contains 0.6% nitrogen in the form of pyridine, amine, pyrrolic and amide groups. The oxidized sample on the other hand contains 2.57 % nitrogen mainly in the form of nitro-type complexes with high binding energies between 405.3–405.9 eV. The latter sample also

contains a smaller amount of nitrogen in the form of pyrroles and amides between 400.1–400.6 eV, pyridines between 398.2–399 eV and finally N-Q in quaternary and/or protonated amines between 401.6–402.2 eV.

The deconvolution of N 1*s* core energy levels (Fig. 3) shows that after ammonia adsorption, the relative concentration of nitrogen in amine groups increased for the exhausted BAX sample. The formation of these groups may be explained through the reaction of ammonia with carbonyl (such as ketones) and epoxy groups. The former reaction is further supported by the deconvolution of O 1*s* core energy levels (Table 5 and Fig. S6 of Supplementary Information), where, the oxygen content in C=O groups decreases. The reaction of ammonia with epoxy groups, would lead to the epoxide ring opening and the formation of $–NH_2$ and -OH groups. This is verified by an increased relative concentration of oxygen in C-O groups (comparison of the deconvolution of O 1*s* core energy levels) and the increased content of nitrogen in amine groups (comparison of the deconvolution of N 1*s* core energy levels). On the surface of the exhausted BAX sample, the relative concentration of pyridine groups decreased compared to the initial BAX. This may be linked to the conversion of some pyridines to aminopyridines after ammonia adsorption and/or the reaction of some anhydride groups of the carbon surface with ammonia, which would lead to the protonation of pyridines (pyridinium), deprotonation of acetic acid and formation of amide groups. The latter reaction is further supported by the increased relative concentration of amide groups and also by the presence of nitrogen in pyridinium groups after exposure to ammonia, as seen from the deconvolution of N 1*s* core energy levels. Finally, the presence of nitrogen in the form of NH_4^+ is the result of acid-base reaction of ammonia with surface carboxylic groups. All of these reactions further support the hypothesis of the higher degree of chemisorption in the case of the initial sample compared to

the oxidized one. Interestingly, based on the deconvolution of N 1*s* core energy levels, it is seen that for the exhausted BAX-O sample the relative concentrations of R-NO_2 and Ph-NO_2 groups increased, which suggests that further extent of oxidation took place on the carbons' surface during the exposure to ammonia.

It was found that oxidation of the initial sample affected its conductivity. As aforementioned, while microchips coated with BAX had a resistance of 68 kΩ, for the oxidized sample the resistance increased considrerably to 1.04 MΩ. This observation is in agreement with the deconvolution of C 1*s* core energy levels (Table 5 and Fig. S5 of the Supplementary Information), where it is seen that after oxidation, the sp^2 C-C contribution decreased notably for BAX-O. In that case the increased content of oxygen and nitrogen results in more defects on the sample's surface and thus resistance to the electron flow.

Table 5. The results of deconvolution of C 1*s*, O 1*s* and N 1*s* core energy levels.

Binding energy, eV	Bond assignment	BAX	BAXE	BAX-O	BAX-OE
C 1*s*					
284.8	C-C (sp^2 carbon) or in nitro compounds	77.86	78.86	68.67	73.75
286.2	C-O, C-H (phenolic, alcoholic, etheric) or C-N, C-NH_2	12.06	12.07	17.40	14.13
287.3	C=O (carbonyl or quinone) or C=N	4.94	4.71	6.98	6.33
288.9	O-C=O (carboxyl or ester)	3.42	2.78	5.53	4.64
290.2	π-π^*	1.72	1.58	1.41	1.15
O 1*s*					
531.6	O=C/ (in carboxyl/carbonyl or N-C-O)	44.43	39.60	16.51	26.82
533.4	O-C/ (in phenol/epoxy or NOx.)	55.57	60.40	83.49	73.18
N 1*s*					
398.2-399	N-6 in Pyridines	41.34	37.68	3.46	6.31
400.1-400.6	N-5 in Pyrrolic, NH amides,C-NH_2	36.56	47.69	9.67	8.01
401.6- 402.2	N-Q in quaternary, NH_4^+, pyridinium		14.63	7.13	2.58
405.3	Oxidized nitrogen functionalities in C-	22.10		79.74	83.09

N^+O-C, Ph-NO_2, R-NO_2 and NO_3^-	

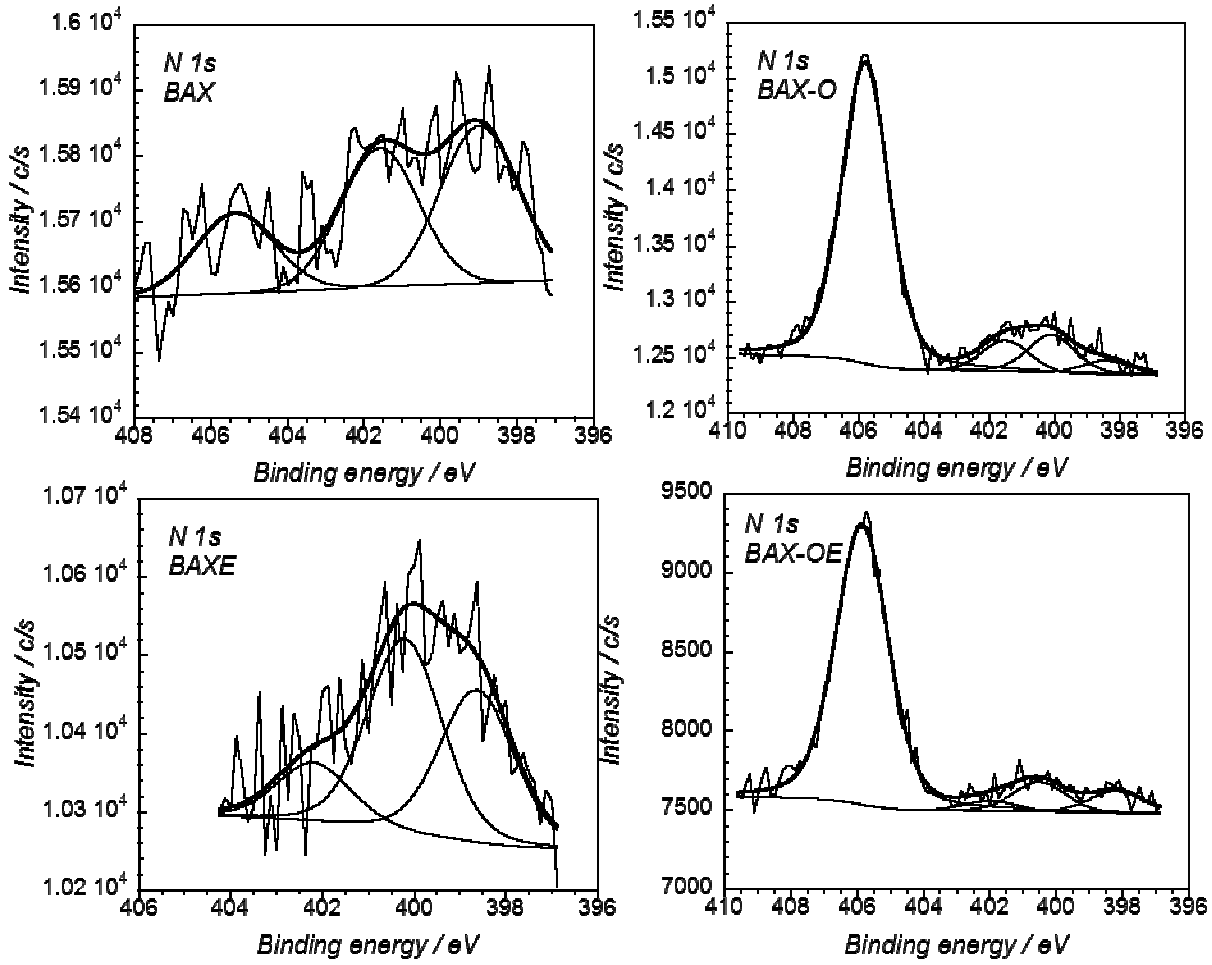

Fig. 3. The deconvolution of N 1*s* core energy levels for the initial and exposed to ammonia oxidized carbons.

Detailed information about the surface acidity, which is expected to affect reactive adsorption of ammonia, is presented in Fig. S7 of Supplementary Information, where pK_a distributions are collected. The results indicate that in the case of BAX, chemical reaction with ammonia changed the surface chemistry, and the presence of NH_4^+ ions is detected at pK_a 9.6. The latter represents reactions of ammonia with carboxylic acids of the surface. In the case of

the oxidized sample, ammonia adsorption leads to the formation of various nitro-type complexes, which is reflected in the high degree of heterogeneity seen in the distributions of the pK_a of surface species.

For sensors recording resistivity changes, the type of charge carriers of the materials is crucial and need to be examined. Therefore, we decided to treat our carbons as semiconductors and to apply the Mott-Schottky approach based on the impedance spectroscopy. Fig. 4 shows the Mott-Schottky plots with the capacitance values of the space region obtained at applied potentials varying from -0.2 V to 1 V. The linear trends with positive and negative slopes indicate the coexistence of both p- and n- type charge carriers in both samples.

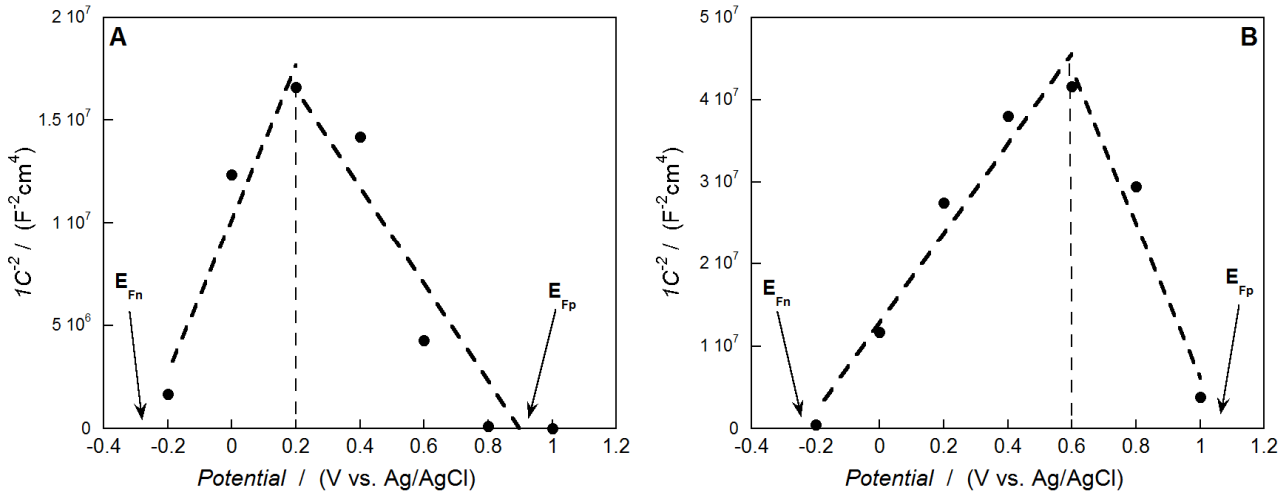

Fig. 4. The Mott-Schottky plot for BAX (A) and BAX-O (B). E_{Fn} and E_{Fp} represent the Fermi levels of n and p type materials.

The x-intercept was used to determine the flatband potential and from the slope of the curve the carrier density was calculated.[42,43] The crossing point of the lines was used as the capacitance values of the space-charge regions. In the Mott-Schottky equation the following dependence is presented:

$$\frac{1}{C^2} = \frac{2}{N_d e \varepsilon_0 \varepsilon}\left(E - E_{FB} - \frac{kT}{e}\right)$$

where, C represents the capacitance of the space-charge region, E and E_{FB} represent the applied potential and Fermi level respectively, ε-the dielectric constant, ε_o - the vacuum permittivity, e - the elementary charge for electrons, N_d -the acceptor or donor density, k - the Boltzmann constant, and T- the absolute temperature. Owing to the small value of the temperature term, it can be neglected. Using this equation with the dielectric constant $\varepsilon = 12$ for activated carbon, the acceptor (N_A) and donor (N_D) densities for BAX were found to be $N_A = 4.86*10^{21}$ and $N_D = 3.38*10^{21}$, respectively. The higher value of N_A indicates that the p-type conductivity is predominant for the BAX sample. For BAX-O on the other hand, the calculated acceptor and donor densities were $N_A = 1.19*10^{21}$ and $N_D = 2.16*10^{21}$, respectively. In that case, the higher value of N_D indicates that the n-type conductivity is predominant for the oxidized sample. These results suggest the change in the carriers' population upon treatment with nitric acid. This kind of treatment was also reported by Vannice and co-workers as leading to the depletion of the concentration of holes in carbon blacks.[46]

Based on the extensive surface characterization of the carbons, the electrical response of the chips and the impedance measurements, a sensing mechanism is proposed for both samples studied. As seen from the impedance measurements, BAX under ambient conditions exhibits both p- and n- type conductivity, with the former one being predominant. It's p-type behavior is related to some degree of disappearance of the π state, because of the bonding between the π- and oxygen-related states, which in turn causes electron transfer from the carbon phase to oxygen.[44] In this case holes play the dominant role in a current transport. Considering that ammonia is an electron donor, the increase in resistance during the reversible exposure to the gas, could be

attributed to the hole depletion of the material, because of the donation of negative charge from ammonia. This in turn makes the activated carbon less p-type, which follows the observed signal change. The increase in resistance during the initial exposure to ammonia is attributed to NH_3 physical adsorption followed by chemical reactions generating the irreversible signal. These reactions may include the formation of amine groups from the reaction of ammonia with carbonyl and epoxy groups, the formation of amide and pyridinium groups from its reaction with surface anhydrides, and also the formation of ammonium salts, resulting from acid-base interactions. Moreover, since this carbon was not fully saturated with oxygen, some surface oxidation by air could also take place. However, the low ammonia breakthrough capacity of BAX (11.5 mg g^{-1}), suggests that chemisorption is not the predominant mechanism. Instead, when the sample is exposed to the challenge gas, electron donation from the physically adsorbed ammonia leads to the depletion of the holes and thus an increase in resistance is observed (Fig. 1A).

BAX-O on the other hand exhibits opposite behavior from that of BAX when initially exposed to ammonia (Fig. 1B). The decrease in the normalized resistance in that case can be explained on the basis of the electronic properties of the activated carbon before and after oxidation. Oxidation of the initial carbon led to its functionalization by nitrogen species, which can be considered as acceptor defects. They can also explain the decrease in the contribution of sp^2 carbon detected from the XPS analysis (Table 5). The presence of these defects, probably contributed to the hole annihilation of the activated carbon sample and its conversion to a predominantly n-type material, as seen from Fig. 4B of the impedance measurements. At the same time oxidation also resulted in the decrease of the material's conductivity.

Besides the change in the conductivity type upon oxidation, another reason for the decrease in the resistance upon ammonia exposure is related to the enhanced physical adsorption in the pore system. Here, the highly polar surface and electron withdrawing NO_2 groups play a crucial role. More precisely, the electric response of the oxidized material may be explained in the context of specific forces that affect physical adsorption of ammonia. These forces include dipole-dipole/hydrogen bonding interactions between the oxygen-functional groups in the pores and ammonia molecules. Hydrogen bonding occurs between NH_3 and hydroxyl groups of carboxylic and phenol groups, either through the coordination of the nitrogen atom in the NH_3 molecule to the hydrogen of the hydroxyl groups (OH···N) or the coordination of one of the three H atoms of NH_3 molecule to the oxygen of the hydroxyl groups (NH···O). The highly polar NO_2 groups also contribute to hydrogen bonding. These weak interactions and the presence of ammonia in the pore system, cause the resistance of the chips to decrease upon exposure to the gas, by providing alternate paths for current conduction across the ultramicropores, through charge hopping.[47] Besides these specific interactions, liquid-like ammonia adsorbed in the very small pores, where functional groups and thus specific interactions cannot exist, also contributes to an increase in DC conductivity, because of the higher conductivity of ammonia compared to that of air.[48] Hence, the sensing performance of BAX-O can be explained on the basis of physical interactions (specific and non-specific) such as hydrogen bonding, polar and dispersive interactions of ammonia with the carbon matrix, and fluid-fluid interactions between quasi-liquid ammonia molecules physically adsorbed in the small pores by a pore-filling mechanism. From Table 1, it is seen that the normalized resistance changes upon exposure to various ammonia concentrations are almost similar for both carbon samples, with BAX exhibiting a slightly greater signal change. The latter, may be linked to the smaller resistance of the BAX coated

microchips, compared to the BAX-O ones. The larger conductivity of the initial sample is apparently related to the carbon in sp^2 C-C configuration and the presence of less defects on its surface. Nevertheless, taking into account the large difference of the resistance between BAX and BAX-O coated chips (6.8 kΩ for BAX and 1.04MΩ for BAX-O), the almost comparable resistance changes upon exposure to ammonia indicate the higher sensitivity of the latter surface.

Our gas sensors were also evaluated in terms of their response time to reach the equilibrium/ a stable response signal when it is exposed to the target gas. At this point we tried to shorten the exposure time of the chips to ammonia, in order to find out if equilibrium could be achieved in a shorter period. From Fig. 5B, it is seen that a sensing cycle for BAX-O could be completed within 4 minutes. However that was not the case for BAX (Fig. 5A), where a sensing cycle was completed within 45 minutes (Fig. 2). That indicates the fast kinetics of ammonia adsorption/desorption on BAX-O. Finally, the response of the sensor was tested for even lower ammonia concentrations, such as 20 ppm and 10 ppm (Fig. 5C and Fig. 5D). From Fig. 5 it is seen that for all ammonia concentrations, the normalized resistance changes are consistent and that the microchips exhibit reversible sensing.

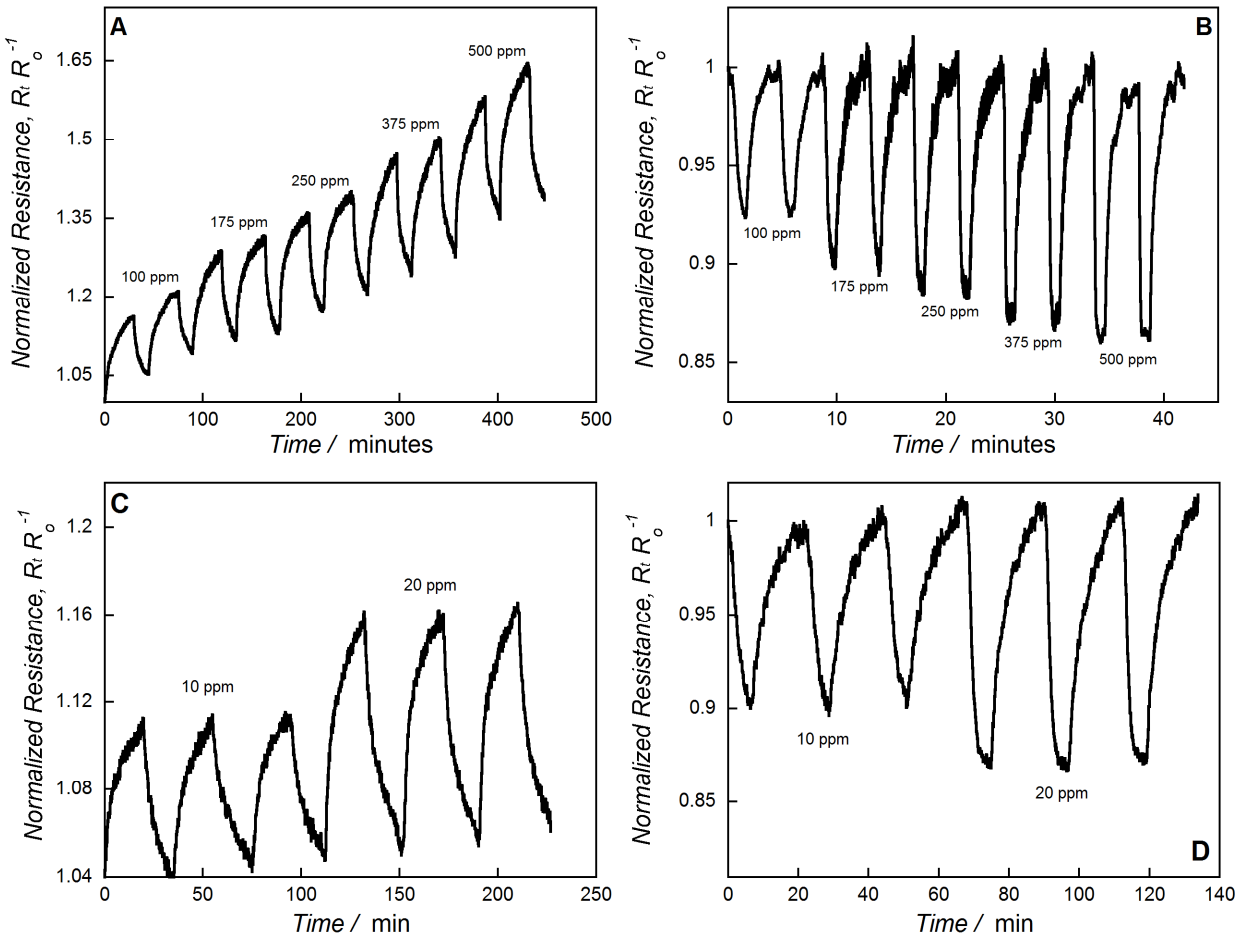

Fig. 5. Response curve for BAX and BAX-O at various ammonia concentrations.

Fig. 6 shows that for both carbon chips, there is a linear trend in the normalized resistance with increasing ammonia concentration. Such a behavior is a desired feature of a gas sensor. The above observation indicates that the sensing mechanism does not change with an increasing the gas concentration. That linearity also indicates that the pores are not filled when carbons are exposed to 500 ppm of ammonia in the challenge gas. A longer exposure time to higher ammonia concentrations would produce a greater signal, because more ammonia would be physically adsorbed in the micropore and mesopore structure, causing a more complete pore

filling. The larger deviation from linearity at concentrations below 100 ppm of ammonia are linked to the larger error on these concentration made by dilution than those over 100 ppm.

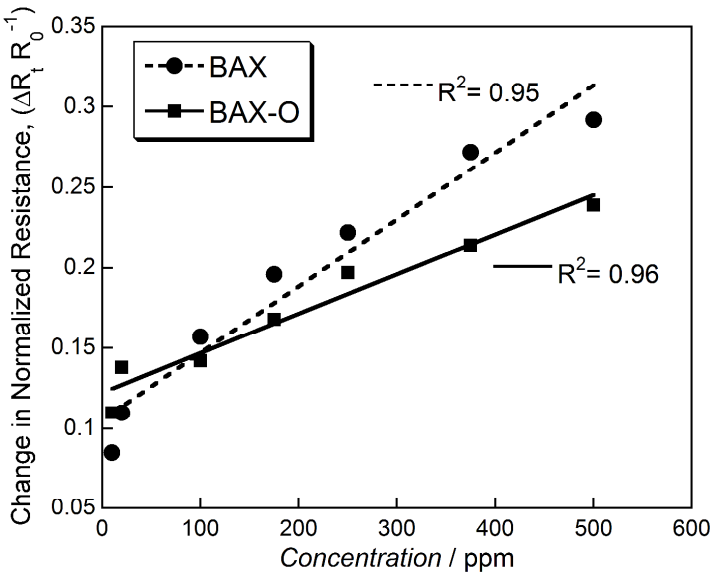

Fig. 6. The dependence of the change in normalized resistance of the studied samples on the ammonia concentration in the challenge gas.

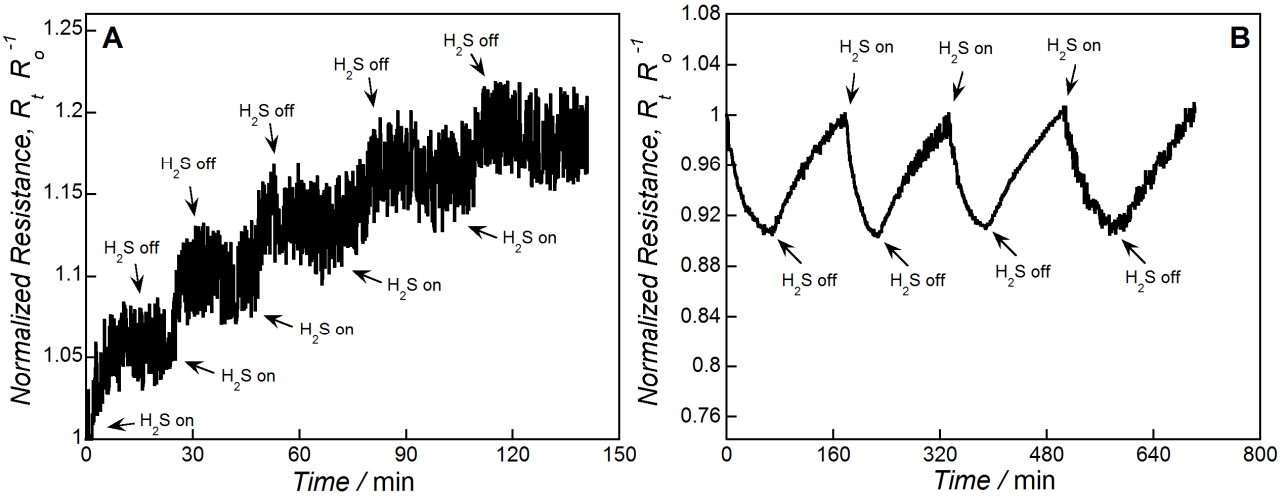

Fig. 7. Response curve for BAX (A) and BAX-O (B) at 500 ppm of H_2S.

To study the sensitivity to reducing gases of different chemistries, the prepared carbon chips were exposed to 500 ppm of H_2S in dry air. The results are summarized in Fig. 7. The BAX and BAX-O chips exhibited 4 and 9 % change in the normalized resistance upon exposure to 500 ppm of H_2S, respectively. We link it to the small adsorption capacities of these carbons[49] owing to the surface acidic properties.[50] Since the changes in the resistivity upon the ammonia exposure at the same conditions were 29.2 and 24.9 % for BAX and BAX-O, respectively (Table 1, these results show the high sensing selectivity toward the ammonia detection of our carbon materials.

Conclusions

The results presented in this paper show that commercial activated carbons can be used as low concentration chemiresistive ammonia sensors. The opposite trends in sensing signal for the initial and oxidized samples indicate that oxidation changes the electrical properties of the material, leading to a different sensing mechanism. In the case of the initial sample, holes play the predominant role in the current transfer hence, exposure to ammonia which is an electron donating gas, would lead to their depletion and thus an increase in resistivity. After oxidation, the carbon surface gets functionalized by oxygen and nitrogen species. The latter in the form of nitro groups, are considered as electron donating, hence contributing to the hole annihilation of the material and its conversion to a predominantly n-type. Therefore, a decrease in resistivity is observed upon ammonia exposure compared to the initial carbon; owing to electron donating properties of ammonia. Physical interactions such as hydrogen bonding, polar interactions with the surface functional groups, and dispersive interactions of ammonia with the carbon matrix led

to pore filling, govern the extent of the response signal. It was shown that the sensing chips exhibit reversible behavior upon exposure to ammonia/air purging and that there is a linear dependence of the electrical response on various ammonia concentrations. These are considered as promising features of a gas sensor. Owing to their porosity and the ability to adsorb ammonia, these sensing chips can also exhibit some protecting properties against ammonia exposure. Testing the chips in H_2S showed a very small response to this gas and thus a high selectivity for ammonia detection.

Experimental

Materials

Commercial-activated carbon of wood origin BAX-1500 (MeadWestvaco) was used in this study. The sample was oxidized with 50 % nitric acid for 5 hours and then washed in Soxhlet apparatus until constant pH of the leachate, to remove the excess of the oxidizing agent and water-soluble compounds. After this procedure, the sample is referred as BAX-O.

Preparation of sensor chips

For the preparation of the sensor, each carbon sample was grounded and made into a slurry using N-methyl-2-pyrrolidinone as solvent, because of its good dispersing properties. The slurry was then spread on to an 8 mm × 8 mm thin-film gold interdigitated electrode, with 50 μm lines/spaces on an alumina substrate, using a blade and finally dried at 120 ^{0}C for 24 hours. Scanning electron micrographs and digital images of the chips before and after coating with the activated carbon slurry are presented in Fig. 8.

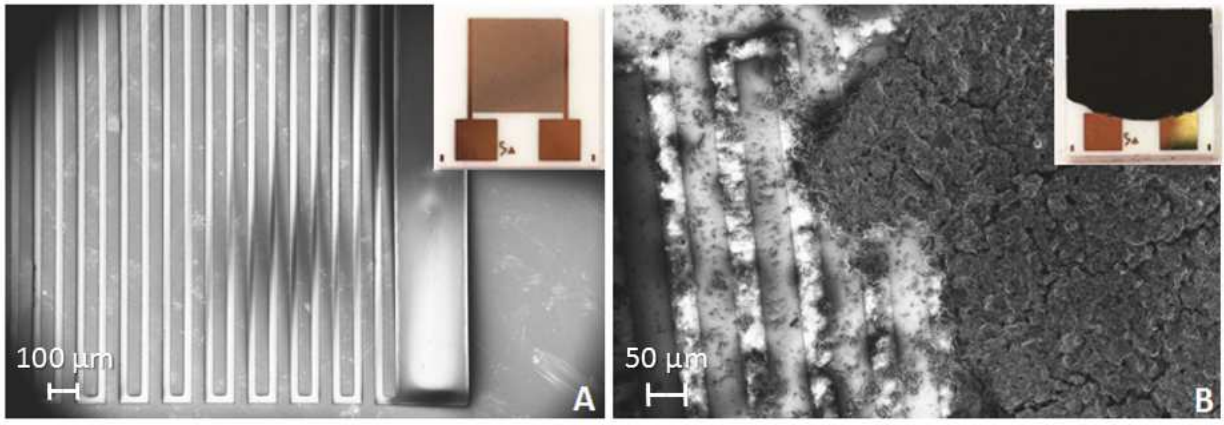

Fig. 8. Scanning electron micrographs and digital images of the chips before coating (A) and after coating (B) with the activated carbon slurry.

Electrochemical measurements

Sensing procedure

For the sensing tests, the activated carbon coated microchips were placed in a 20 cm^3 home-made gas chamber which was purged with dry air to establish dynamic equilibrium. The Electrical measurements and sensing performance were monitored using a VersaSTAT MC (AMETEK, Princeton Applied Research) via four-wire sensing at room temperature, while a 1V voltage was applied.

The chips were initially purged with dry air until the electrical signal stabilized. Then they were exposed to ammonia, flowing at 500 ml min^{-1}, until the signal reached a steady state. Next, the chips were again purged with air to remove physically adsorbed ammonia and determine the role of chemisorption (irreversible processes) and porosity on the sensing signal.

Such treated chips were further tested for sensing via reversible processes, by exposing them to 10, 20, 100, 175, 250, 375 and 500 ppm of ammonia followed by purging with air.

From the data obtained, the normalized resistance ($R_t\ R_o^{-1}$) of the chips was calculated, where R_o and R_t are the resistance of the sensor initially, and at any time, *t*, during exposure to ammonia respectively.

To test the selectivity of response to other reducing gases of different chemistry, the carbon chips were exposed to 500 ppm of H_2S in dry air. The experiments were run following the steps applied for ammonia sensing.

Impedance measurements

The impedance spectroscopy was carried out in 0.5 M Na_2SO_4, in a three-electrode cell, using a Ag/AgCl (3M KCl) as the reference electrode, the active material as the working electrode, and a platinum rod as the counter electrode. The working electrode was prepared by coating a Ti foil collector of active area of $1cm^2$, with the well-grounded slurry of the activated carbon and polyvinylidene fluoride (PVDF) (ratio 90:10) in N-methyl-2- pyrrolidinone (NMP). The electrodes were dried at 120 °C for 24 hour. Potentiostatic electrochemical impedance spectroscopy (EIS) measurements were performed using VersaSTAT MC (AMETEK, Princeton Applied Research) in the frequency range of 0.05 Hz – 100 kHz with a 10 mV AC amplitude, at various potential vs reference electrode, ranging from -0.2 V to 1.0 V.

Methods

NH_3 breakthrough dynamic test. Ammonia breakthrough capacity was measured in dynamic conditions, at room temperature, using a laboratory designed test. For the former, adsorbent samples were packed into a glass column (length 370 mm, internal diameter 9 mm).

The bed volume used was about 2 cm^3 (with particles having size 1 mm and 2 mm). The total flow rate of the inlet stream was 225 mL min^{-1} with an ammonia concentration of 1000 ppm.

Ammonia breakthrough was monitored using an electrochemical sensor (Multi-Gas Monitor ITX system). The challenge gas flow was arbitrarily stopped at the breakthrough concentration of 100 ppm. The adsorption capacity of each adsorbent was calculated by integration of the area above the breakthrough curve taking into account the ammonia concentration in the inlet gas, the flow rate, the breakthrough time, and the mass of a sorbent used. Error in the adsorption capacity is estimated to be about 10–15%.

Sorption of Nitrogen. On the materials obtained, sorption of nitrogen at its boiling point was carried out using ASAP 2020 (Micromeritics). Before the experiments, the samples were outgassed at 120 °C to constant vacuum (10^{-4} kPa). From the isotherms, the surface areas (NLDFT method), total pore volumes, V_t (from the last point of isotherm at a relative pressure equal to 0.99), volumes of micropores, V_{mic}, mesopore volume, V_{mes}, along with pore size distributions were calculated from the isotherms. Non – Local Density Functional Theory (NLDFT) was used to calculate the pore size distributions (free download at www.nldft.com).[51,52]

SEM. Scanning electron microscopy (SEM) images were obtained with a Zeiss Supra 55 VP. The accelerating voltage was 5.00 kV. Scanning was performed in situ on a sample powder without coating.

Raman spectroscopy. Raman spectra were collected on a MonoVista Confocal Raman microscope spectrometer using a 514.5 nm argon ion laser. The experiments were done on the powdered samples deposited on a silicon wafer.

XPS. The elements present in the materials studied as well as their chemical state were identified by X-ray photoelectron spectroscopy (XPS) analysis. A Physical Electronics spectrometer (PHI 5700) was used with MgKα X-ray radiation (1253.6 eV) as the excitation source. High resolution spectra were recorded at a take-off angle of 45° by using a concentric hemispherical analyzer operating in constant-pass-energy mode at 29.35 eV, with a 720 μm diameter analysis area.

Potentiometric titration. Potentiometric titration measurements were performed with a DMS 888 Titrando automatic titrator (Metrohm). The instrument was set at the mode when the equilibrium pH was collected. Subsamples of the materials studied of about 0.100 g in 50 mL $NaNO_3$ (0.01 M) were placed in a container maintained at 25 ^oC and equilibrated overnight with the electrolyte solution. To eliminate the influence of atmospheric CO_2, the suspension was continuously saturated with N_2. The suspension was stirred throughout the measurements. Volumetric standard NaOH (0.1 M) was used as the titrant. The experiments were done in the pH range of 3–10. Each sample was titrated with base after acidifying the sample suspension.

The experimental data were transformed into a proton binding isotherm, Q, representing the total amount of protonated sites, which is related to the pK_a distribution by the integral equation[53] whose solution was obtained using the numerical procedure applying regularization combined with non-negativity constraints [40]. Based on the spectrum of acidity constants and the history of the samples, the detailed surface chemistry was evaluated.

CHN analysis. Elemental chemical analysis was performed with a LECO CHNS 932 analyzer.

Acknowledgements

This work was supported by the ARO (Army Research Office) grant W911NF-10-1-0030 and W911NF-13-1-0225, and NSF collaborative SBET Grant No. 1133112. Special thanks are addressed to Kavindra Singh for his experimental advice as well as to Omar Green for his help in Raman experiments.

References:

1. J. Phillips, *Control Technology Center U.S. Environmental Protection Agency*, EPA Contract No. 68-D1-0073, Work Assignment No. 3-39 Vienna, 1995.

2. B. Timmer, W. Olthuis, A. Van Den Berg, *Sens. Actuators B: Chem.*, 2005, **107**, 666–677.

3. C. Plog, A. Knezevic, H. Leye, R. Moos, R. Mu, E. Irion, T. Braun, *Sens. Actuators B: Chem.*, 2002, **83**, 181–189.

4. J. Guo, W. S. Xu, Y. L. Chen, A. C. Lua, *J. Coll. Interf. Sci.*, 2005, **281**, 285–90.

5. *Toxicological profile for ammonia*, U.S. Deartment of health and human services, Public Health Service, Agency for Toxic Substances and Disease Registry, 2004.

6. Hazards of Ammonia Releases at Ammonia Refrigeration Facilities (Update). United States Environmental Protection Agency, EPA, 550-F-01-009, 2001.

7. CDC online, NIOSH, http://www.cdc.gov/niosh/idlh/7664417.html (accessed October 2014)

8. Y.-S. Lee, K.-D. Song, J.-S. Huh, W.-Y. Chung, D.-D. Lee, *Sens. Actuators B: Chem.*, 2005, **108**, 292–297.

9. T. Hibbard, K. Crowley, F. Kelly, F. Ward, J. Holian, A. Watson,A. J. Killard, *Anal. Chem.*, 2013, **85**, 12158–65.

10. X. Liu, S. Cheng, H. Liu, S. Hu, D. Zhang, H. Ning, *Sensors (Basel).*, 2012, **12**, 9635–65.

11. P. Teerapanich, M. T. Z. Myint, C. M. Joseph, G. L. Hornyak, and J. Dutta, *IEEE Trans. Nanotechnol.* , **12**, 255–262.

12. S. Yoo, X. Li, Y. Wu, W. Liu, X. Wang and W. Yi, *J. Nanomater.*, 2014, **2014**, 1–6.

13. S. Some, Y. Xu, Y. Kim, Y. Yoon, H. Qin, A. Kulkarni, T. Kim, H. Lee, *Sci. Rep.*, 2013, **3**, 1868.

14. A. Lipatov, A. Varezhnikov, P. Wilson, V. Sysoev, A. Kolmakov, A. Sinitskii, *Nanoscale*, 2013, **5**, 5426–34.

15. J. T. Robinson, F. K. Perkins, E. S. Snow, Z. Wei, P. E. Sheehan, *Nano Lett.*, 2008, **8**, 3137–40.

16. E. C. Mattson, K. Pande, M. Unger, S. Cui, G. Lu, M. Weinert, J. Chen, C. J. Hirschmugl, *J. Phys. Chem. C,* 2013, **117** (20), 10698–10707.

17. J.-M. Tulliani, A. Cavalieri, S. Musso, E. Sardella and F. Geobaldo, *Sens. Actuators B: Chem.*, 2011, **152**, 144–154.

18. Y. Wang, L. Zhang, N. Hu, Y. Wang, Y. Zhang, Z. Zhou, Y. Liu, S. Shen, C. Peng, *Nanoscale Res. Lett.*, 2014, **9**, 251.

19. X. Huang, N. Hu, R. Gao, Y. Yu, Y. Wang, Z. Yang, E. Siu-Wai Kong, H. Wei, Y. Zhang, *J. Mater. Chem.*, 2012, **22**, 22488.

20. N. Hu, Z. Yang, Y. Wang, L. Zhang, Y. Wang, X. Huang, H. Wei, L. Wei, Y. Zhang, *Nanotechnol.*, 2014, **25**, 025502.

21. L. Q. Nguyen, P. Q. Phan, H. N. Duong, C. D. Nguyen,L. H. Nguyen, *Sensors (Basel).*, 2013, **13**, 1754–62.

22. E. C. Jesús, J. Li, C. R. Cabrera, in *Syntheses and Applications of Carbon Nanotubes and Their Composites,* in *Syntheses and Applications of Carbon Nanotubes and Their Composites,* ed. Satoru Suzuki, InTech, 2013, ch. 15.

23. A. Abdelhalim, A. Abdellah, G. Scarp, P. Lugli, *Nanotechnol.*, 2014, **25**, 055208.

24. R. Mangu, S. Rajaputra , V. P. Singh, *Nanotechnol.*, 2011, **22**, 215502.

25. H. Vedala, D. C. Sorescu, G. P. Kotchey, A. Star, *Nano Lett.,* 2011, **11** (6), 2342–2347.

26. Y. Wang, L. Zhang, N. Hu, Y. Wang, Y. Zhang, Z. Zhou, Y. Liu, S. Shen, C. Peng, *Nanoscale Res. Lett.*, 2014, **9**, 251.

27. S. Fung, Y. W. Zhao, C. D. Beling, X. L. Xu, N. F. Sun, T. N. Sun, X. D. Chen, *J. Appl. Phys.*, 1999, **86**, 2361.

28. X. Wang, X. Li, L. Zhang, Y. Yoon, P. K. Weber, H. Wang, J. Guo, H. Dai, *Science*, 2009, **324**, 768–71.

29. M. Gonçalves, L. Sánchez-García, E. De Oliveira Jardim, J. Silvestre-Albero, F. Rodríguez-Reinoso, *Environ. Sci. Technol.*, 2011, **45**, 10605–10.

30. M. Seredych, D. Hulicova-Jurcakova, G. Q. Lu,T. J. Bandosz, *Carbon,* 2008, **46**, 1475–1488.

31. E. Frackowia, F. Béguin, *Carbon*, 2001, **39**, 937–950.

32. G. Pandolfo, F. Hollenkamp, *J. Power Sour.*, 2006, **157**, 11–27.

33. S. Manocha, N. Movaliya, *Carbon Lett.*, 2007, **8**, 17–24.

34. Jae Hyuck Kwon , Ph.D. Thesis, University of Saskatchewan, 2007.

35. K. Singh, N. A. Travlou, S. Bashkova, E. Rodríguez-Castellón, T. J. Bandosz, *Carbon*, 2014, **80**, 183-192.

36. L. M. Le Leuch, T. J. Bandosz, *Carbon*, 2007, **45**, 568–578.

37. F. Yavari, Z. Chen, A. V. Thomas, W. Ren, H.-M. Cheng, N. Koratkar, *Sci. Rep.*, 2011, **1**, 166.

38. M. Gautam, A. H. Jayatissa, *Solid. State. Electron.*, 2012, **78**, 159–165.

39. Y. Wang, L. Zhang, N. Hu, Y. Wang, Y. Zhang, Z. Zhou, Y. Liu, S. Shen, C. Peng, *Nanoscale Res. Lett.*, 2014, **9**, 251.

40. J. Jagiello, T. J. Bandosz, J. A. Schwarz, *Carbon*, **32**, 1026–1028.

41. C. Petit, K. Kante, T. J. Bandosz, *Carbon*, 2010, **48**, 654–667.

42. M. G. S. Ferreira, G. Engineering, *J. Braz. Chem. Soc.*, 2002, **13**, 1–14.

43. Y. Wang, C. Chang, T. Yeh, Y. Lee, H. Teng, *J. Mater. Chem. A*, 2014, **2**, 20570-20577 .

44. H. K. Jeong, C. Yang, B. S. Kim , K. Kim, *EPL (Europhysics Lett.)*, 2010, **92**, 37005.

45. P. T. Araujo, M. Terrones, M. S. Dresselhaus, *Mater. Today*, 2012, **15**, 98–109.

46. Chan-Chiung Liu, A.B. Walters, M.A. Vannice, *Carbon* 1995, **33**, 1699–1708.

47. J. S. Im, S. C. Kang, S.-H. Lee , Y.-S. Lee, *Carbon*, 2010, **48**, 2573–2581.

48. D. R. Lide, ed., *CRC Handbook of Chemistry and Physics*, Internet Version 2005, http://www.hbcpnetbase.com, CRC Press, Boca, Raton, FL, 2005.

49. M. Seredych, T. J. Bandosz, *Energy Fuels*, 2008, **22**, 850–859.

50. T. J. Bandosz, *J. Coll. Interf. Sci.*, 2002, **246**, 1–20.

51. J. Jagiello, J. P. Olivier, *Carbon*, 2013, **55**, 70–80.

52. J. Jagiello, J. P. Olivier, *Adsorption*, 2013, **19**, 777–783.

53. J. Jagiello, *Langmuir*, 1994, **10**, 2778–2785.

Captions to the Tables

Table 1. Change in the normalized resistance ($R_t R_o^{-1}$) of BAX and BAX-O after exposure to various ammonia concentrations.

Table 2. Ammonia breakthrough capacity and surface pH values.

Table 3. The parameters of porous structure for BAX and BAX-O before and after exposure to ammonia.

Table 4. Content of elements on the surface (in at. % from XPS analysis and in wt. % from CHN analysis).

Table 5. The results of deconvolution of C 1*s*, O 1*s* and N 1*s* core energy levels.

Captions to the Figures

Fig. 1. Normalized change in resistance of BAX (A) and BAX-O (B) upon initial exposure to ammonia and subsequent purging with air after stabilization.

Fig. 2. Response curve for BAX (A) and BAX-O (B) both at various ammonia concentrations.

Fig. 3. The deconvolution of N 1*s* core energy levels for the initial and exposed to ammonia oxidized carbons.

Fig. 4. The Mott-Schottky plot for BAX (A) and BAX-O (B). E_{Fn} and E_{Fp} represent the Fermi levels of n and p type materials.

Fig. 5. Response curve for BAX and BAX-O at various ammonia concentrations.

Fig. 6. The dependence of the change in normalized resistance of the studied samples on the ammonia concentration in the challenge gas.

Fig. 7. Response curve for BAX (A) and BAX-O (B) at 500 ppm of H_2S.

Fig. 8. Scanning electron micrographs and digital images of the chips before coating (A) and after coating (B) with the activated carbon slurry.